Laser and Particle Beams (2007), *25*, 425–433. Printed in the USA.

DOI: 10.1017/S0263034607000547

Interferometric investigations of influence of target irradiation on the parameters of laser-produced plasma jets

A. KASPERCZUK,[1] T. PISARCZYK,[1] S. BORODZIUK,[1] J. ULLSCHMIED,[2] E. KROUSKY,[3] K. MASEK,[3] M. PFEIFER,[2] K. ROHLENA,[3] J. SKALA,[3] AND P. PISARCZYK[4]

[1]Institute of Plasma Physics and Laser Microfusion, Warsaw, Poland
[2]Institute of Plasma Physics AS CR, Prague, Czech Republic
[3]Institute of Physics AS CR, Prague, Czech Republic
[4]Warsaw University of Technology, Warsaw, Poland

(RECEIVED 8 February 2007; ACCEPTED 10 May 2007)

Abstract

Our recent experimental results demonstrate that the formation of plasma jets is a fundamental process accompanying the laser produced plasma expansion, if a massive planar target with relatively high atomic number is irradiated by a defocused laser beam. In this paper some new results on the influence of target irradiation conditions on plasma jet parameters are presented. The experiment was carried out at the PALS iodine laser facility, with the third harmonic beam of the pulse duration of 250 ps (FWHM). The beam energies varied in the range of 13–160 J, the focal spot radii in the range of 35–600 μm. The planar massive targets used in the experiment were made of Cu, Ag and Ta. For measurements of the electron density evolution a three frame interferometric system was employed. The jets were observed in the whole range of the laser energy used. The initial velocities of the plasma jets produced in the reported experiment reached the value of up to $7 \cdot 10^7$ cm/s, the jets were up to 4 mm long including the jet pedestal and about 400 μm in diameter. Calculations of the efficiency of the plasma jet production show that it decreases with increasing the laser energy.

Keywords: Efficiency of plasma jet production; Electron density; Interferometric system; Plasma jet; Target irradiation

1. INTRODUCTION

The high-Mach-number jets are ubiquitous in nature. Highly collimated jets originating from different astrophysical processes represent a subject of particular interest (Schopper, 2003; Ampleford *et al.*, 2005; Bellan, 2005). As it has been shown in recent laboratory experiments with high-power lasers, in the multi-shell target geometry, the contact surfaces of different materials may induce formation of multiple shocks, and, also, of plasma jets (Goldman *et al.*, 1999; Blue *et al.*, 2005; Andreev, 2004). Therefore, the investigation of supersonic plasma jets production in laboratory conditions becomes a fundamental issue in both the astrophysical and the inertial confinement fusion contexts. Such experiments could deliver essential information on the mechanisms of jet generation and would allow testing the validity of numerical algorithms and physical models.

The first successful attempts to generate laboratory plasma jets relevant to astrophysical observations are described for example, in the papers of Farley *et al.* (1999) and Shigemori *et al.* (2000). Conically shaped targets made of different materials were irradiated by five beams of the Nova laser with pulse duration of 100 ps and energy in each beam of 225 J, or by six beams of the GEKKO-XII laser with the same pulse duration, but with the total energy of 500 J. The jet-like structures were formed by collisions of the ablated flows at the axis of conical targets. Plasma jets are also considered in fast ignition scenarios (Velarde, 2005). Therefore, a number of experimental and theoretical works is devoted to investigate the details of plasma jet formation (Schaumann, 2005; Sizyuk *et al.*, 2007).

Recently, we have demonstrated a simple method of jet production by interaction of a relatively low-energy laser pulse with a massive planar metallic target (Kasperczuk *et al.*, 2006). That experiment was carried out at the PALS iodine laser facility (Jungwirth, 2005). Successful realization of the plasma jet generation required a target material with the atomic number greater than that of aluminum, a short wavelength, and a relatively large focal spot radius. Numerical simulations of the plasma dynamics related to the experimental data, performed by using the laser-plasma

Address correspondences and reprint requests to: Tadeusz Pisarczyk, Institute of Plasma Physics and Laser Microfusion, 23 Hery Street, 00-908 Warsaw, Poland. E-mail: pisaro@ifpilm.waw.pl

interaction hydrodynamic code FCI2 (Nicolai *et al.*, 2006), have shown that the fast radiative cooling of plasma, which starts before the expansion process, plays a crucial role at launching the jet and its collimation.

Since the results presented in the paper by Kasperczuk *et al.* (2006) were obtained at somewhat arbitrarily chosen target irradiation conditions (the laser energy of 100 J and the focal spot radius of 300 μm with the focal point located inside of the target), it seemed to be of interest to test the possibility of the plasma jet generation under different conditions, by varying both the focal spot radius and the laser energy over wide ranges. Moreover, determination of the optimum target irradiation conditions for the plasma jet production becomes very important in the context of our subsequent investigations of the interaction of a plasma jet with a slowly moving cloud of gas or plasma. The current experiment was performed with the third harmonic of the laser frequency, as the parameters of the jets were better for this harmonic than for the first one (Kasperczuk *et al.*, 2006). The planar massive targets used were made of metals of largely different atomic numbers—Cu, Ag, and Ta.

2. EXPERIMENTAL SET-UP

For studying the temporal and spatial behaviors of the plasma expansion a three-frame laser interferometric system was used. In order to get electron density distributions, the methodology described in the paper Kasperczuk and Pisarczyk (2001) was employed.

The experimental investigations were carried out at the PALS iodine laser facility (Jungwirth *et al.*, 2001, 2005; Batani, 2007). The planar massive targets were made of three materials with different atomic numbers, Cu ($Z = 29$), Ag ($Z = 47$), and Ta ($Z = 73$). The laser provided a 250 ps (FWHM) pulse with the energies in the range of 13–160 J at the third harmonic frequency ($\lambda_3 = 0.438$ μm). The full laser beam diameter at the target chamber entrance window was about 290 mm. Inside of the chamber; the beam was focused by means of an aspherical lens with a focal length of 600 mm. By changing the lens position relative to the target, the focal spot radius at the planar massive target was adjusted to 35, 200, 300, 400, 500, and 600 μm (the focal point was located inside the target). In each laser shot, the laser intensity distribution over the laser beam cross-section was recorded by using a CCD camera. To avoid diffraction effects, which could disturb the laser beam intensity distribution on the target surface, retransmission of the beam on the target through a soft diaphragm placed in the laser system, as well as a proper space beam filtration were used.

The plasma expansion was studied by means of a three-frame laser interferometric system with automatic image processing. Each of the interferometric channels was equipped with an independent interferometer of the folding-wave type. The interferometers exploited a blue diagnostic laser beam, which was created by a split-off part of the main infrared laser beam, converted subsequently to the third harmonic frequency. The delay between the interferometric frames was set up to 3 ns.

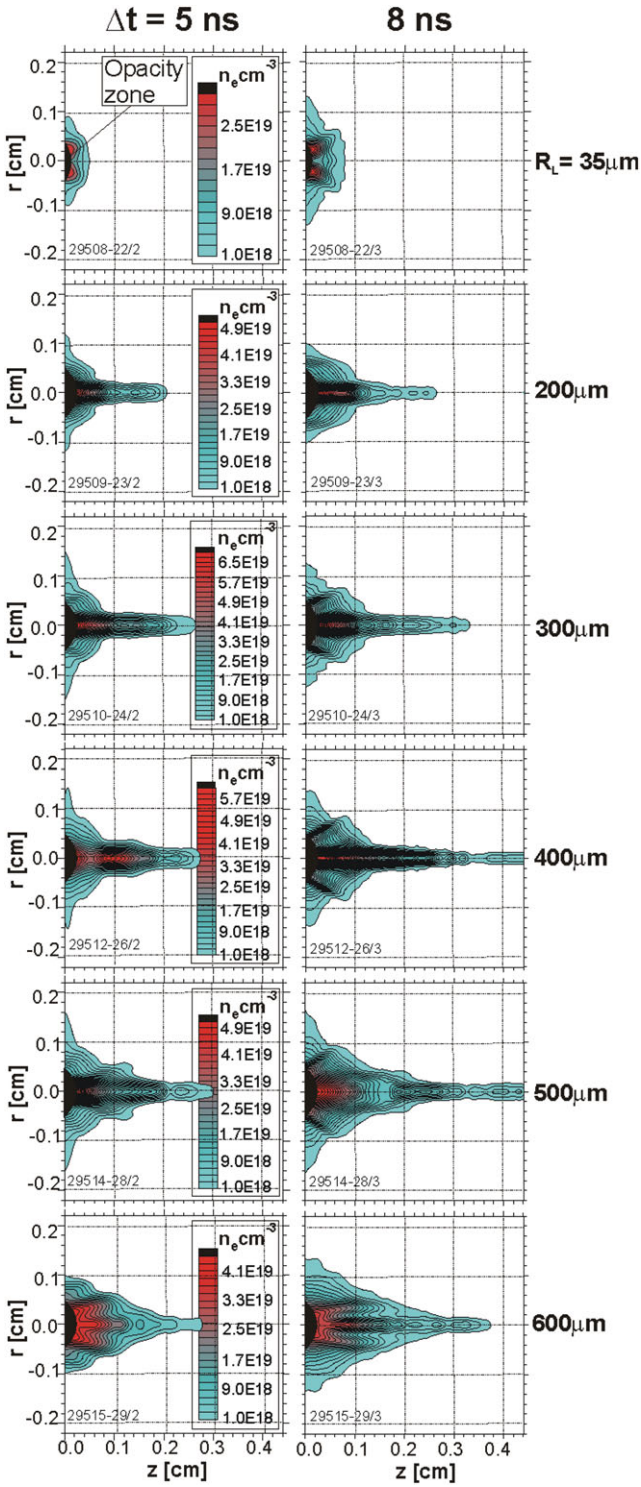

Fig. 1. The Ag plasma configurations at $\Delta t = 5$ ns and $\Delta t = 8$ ns, for the laser energy of 100 J and various focal spot radii.

https://doi.org/10.1017/S0263034607000547 Published online by Cambridge University Press

3. INFLUENCE OF THE FOCAL SPOT RADIUS ON THE PLASMA JET PARAMETERS

This testing was performed at the laser energy of 100 J, for all the target materials. The plasma distributions versus the focal spot radius for those three metals were qualitatively similar. Thus, in order to illustrate the focal spot radius influence on the plasma jet parameters, just the results of interferometric measurements obtained for the Ag target are shown here. In Figure 1, the plasma configurations at $\Delta t = 5$ ns and $\Delta t = 8$ ns, and at various focal spot radii are presented. At that period the plasma jets take their final form. In all the diagrams, the plasma stream boundary is represented by the electron density contour $n_e = 10^{18}$ cm^{-3}. The step of all the adjacent equidensity lines is $\Delta n_e = 2 \times 10^{18}$ cm^{-3}.

One can see that for the smallest focal spot radii, the electron density distributions have a strong depression on the axis. Therefore, in such cases, there is no possibility of the plasma jet creation. For all the materials used, the jet forming starts at the focal spot radius (R_L) close to 200 μm. The observed elongated plasma structure propagates along the axis with an initial velocity reaching the maximum value of 7×10^7 cm/s (the velocity was determined on the basis of the jet front position after 5 ns). On the basis of our investigations, one can ascertain that the longest plasma jets with the smallest diameters are formed at $R_L = 300$ μm. The shapes of plasma jets for R_L and for all of the target materials are shown in Figure 2. The jets travel over a distance of up to 4 mm, whereas their diameters vary from 0.7 mm for the lightest target material (Cu) down to 0.4 mm for the heavy ones. When increasing R_L above 300 μm the jet radius grows up and, finally, for $R_L =$ 600 μm the jet pedestal becomes divided into a central jet and an outer quasi-cylinder. Quite naturally, at the greatest focal spot radii suitable conditions occur for creating more complex plasma configurations.

Explanation of the absence of plasma jets in the case of the smallest focal spot radii can be found in the paper by Nicolai et al. (2006), where a theoretical analysis of jet formation is presented. In particular, when going to smaller R_L, the

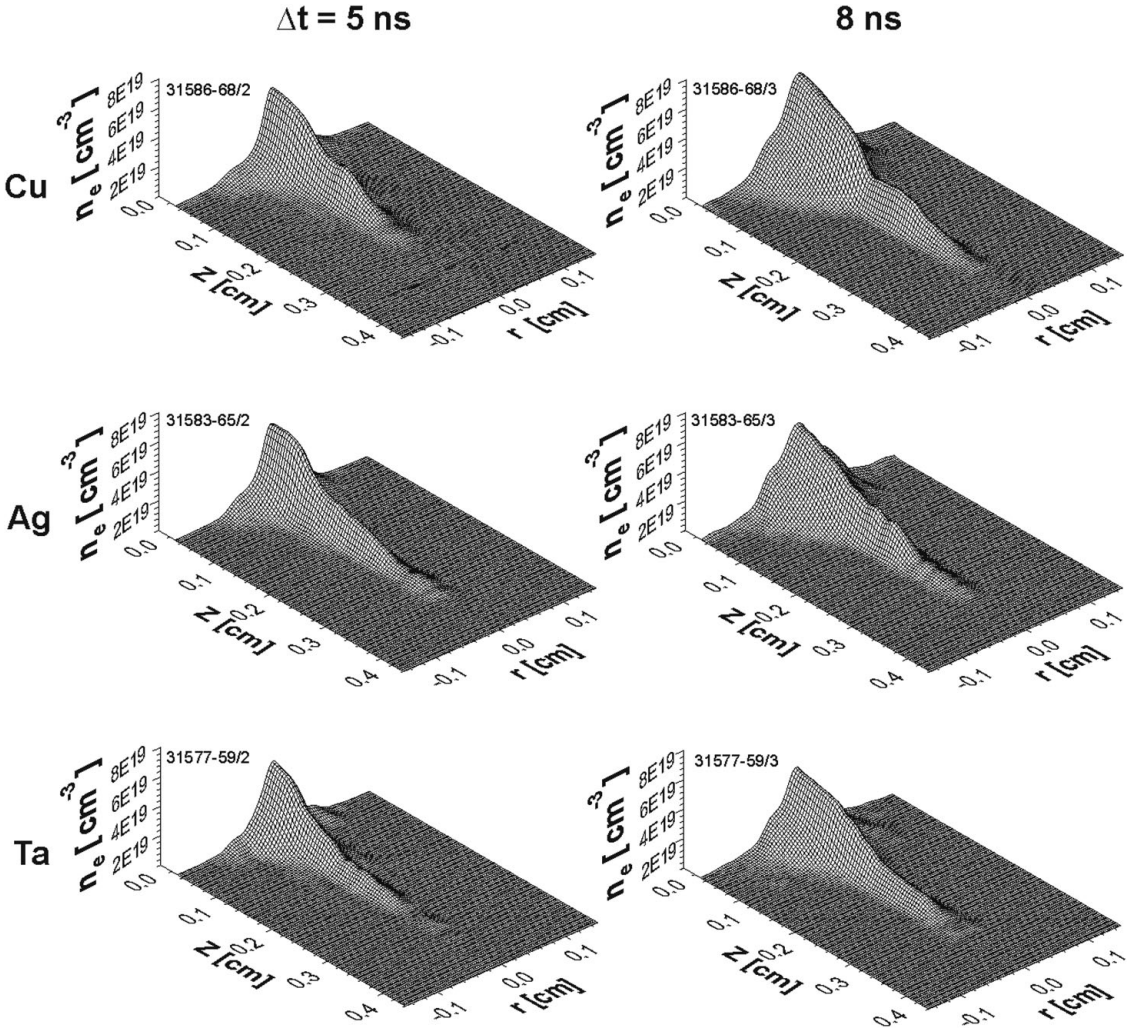

Fig. 2. The structures of the plasma jets at $\Delta t = 5$ and 8 ns for the focal spot radius of 300 μm and three different target materials.

https://doi.org/10.1017/S0263034607000547 Published online by Cambridge University Press

conditions for plasma jet generation gradually deteriorate, since with decreasing R_L the plasma expands with a higher velocity, due to the growing plasma temperature. The conical plasma outflow for $R_L = 35$ μm, seen in Figure 1, results from a faster decay of the central plasma because of its much higher velocity in comparison with that at the plasma periphery. Under these conditions, the characteristic hydrodynamic time (t_h) associated with the plasma expansion becomes shorter than the time of radiation cooling (t_r), which is responsible for the plasma jet formation. For the typical parameters of the experiment at $R_L = 300$ μm, the hydrodynamic time and the radiation cooling time are $\Delta t_h \sim 6$ ns and $\Delta t_r \sim 0.9$ ns, respectively. On the contrary, already for $R_L = 100$ μm, the hydrodynamic time becomes shorter ($t_h \sim 1$ ns) than the radiation time ($t_r \sim 1.2$ ns).

4. INFLUENCE OF THE LASER ENERGY ON THE PLASMA JET CHARACTERISTICS

Since the above results have shown that the focal spot radius of 300 μm seems to be optimum for the plasma jet generation, that radius was chosen for further investigations. In order to determine the influence of laser energy on the properties of plasma jets, the laser energy was varied over a wide range. The possibility of plasma jet generation at low energies was tested by adjusting the laser energy to the lowest possible value of 13 J. For the other measurements, the energies of 50, 120, and 160 J were chosen.

The sequences of the electron density distributions for all the target materials in Figures 3, 4, and 5, show that the capability of the plasma jet forming does not depend on the laser energy. For all the energies used in the experiment

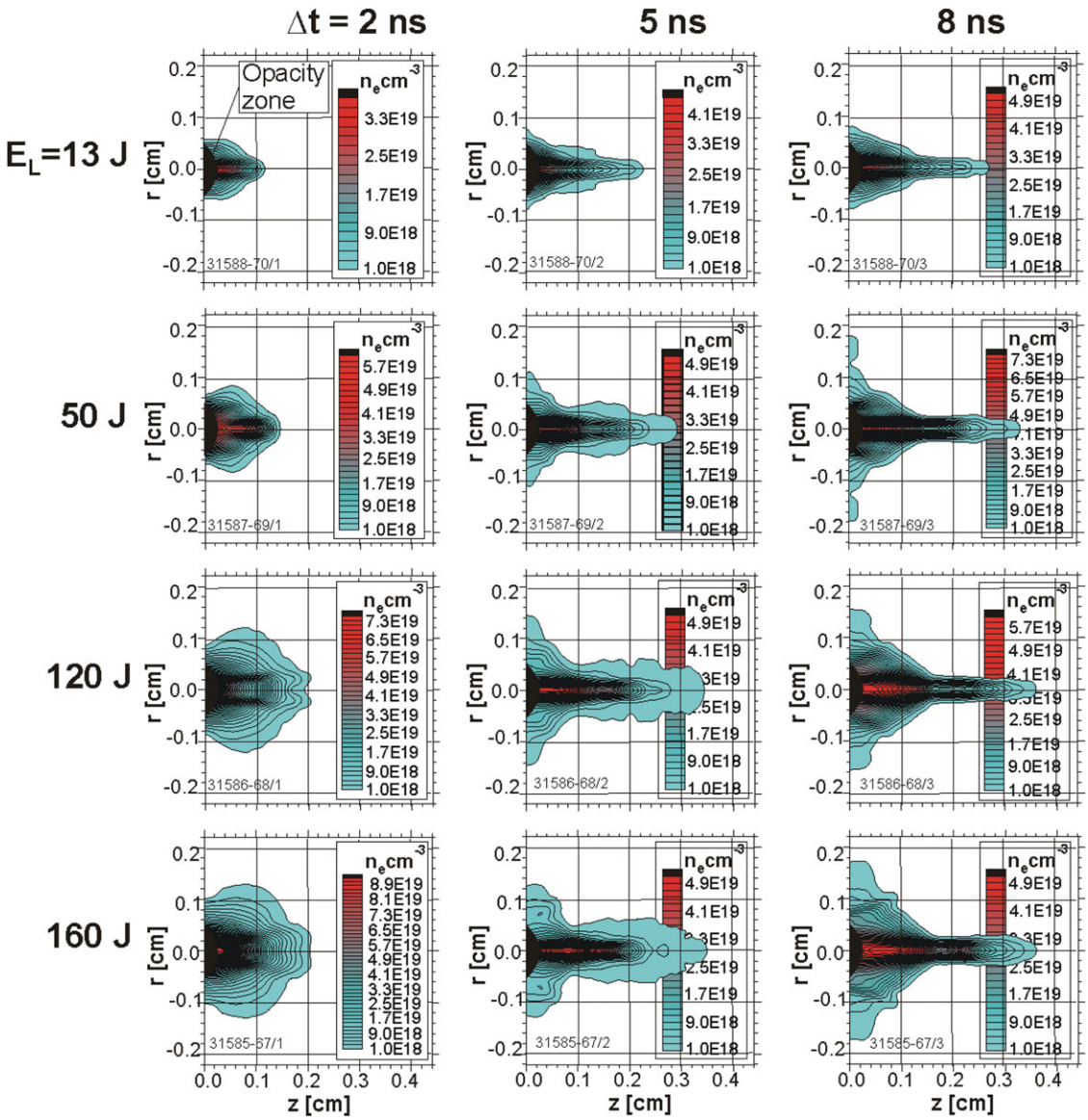

Fig. 3. Sequences of electron isodensitograms at the plasma jet forming stage. The Cu target and various laser energies.

https://doi.org/10.1017/S0263034607000547 Published online by Cambridge University Press

the parameters of the plasma jets produced under the same target irradiation conditions have well reproducible parameters. The dependence of the jet velocity, diameter and electron density on the laser energy is weak; the values of these parameters do not differ too much even for the minimum and maximum energy values.

The plasma jet forming starts very early. A distinct plasma jet configuration is well seen already at $\Delta t = 2$ ns. The plasma jet propagates axially, starting with the velocity of $(3-4) \times 10^7$ cm/s for the lowest energy and $(6-7) \times 10^7$ cm/s for the highest one. Later on the jet velocity decreases rapidly, so the plasma jet forming becomes more or less stationary (see Kasperczuk *et al.*, 2006). Meaning that, in spite of the plasma motion, the jet configuration seems to be at rest. However, the plasma jet forming in the case of the Cu target, at the highest laser energies runs differently. At $\Delta t = 2$ ns, instead of an axial jet, a conical plasma configuration is observed. Next, that configuration collapses on the axis and a typical jet appears. Taking into account that the plasma jet forming results from the radiative cooling, one can infer that the dense plasma collapse is induced by compression of the outer thin, but hot, plasma envelope. After the collapse, the plasma plume consists of a plasma jet and a plasma background, which surrounds the jet (see Fig. 3, $\Delta t = 5$ ns). This latter plasma configuration, however, disappears very fast, being not visible already at $\Delta t = 8$ ns. The plasma background seems to be created by some remainder after the dense plasma collapse. It is a question why in the case of the highest laser energies, the Cu jet forming lasts longer, running through the collapse stage, whereas for the other cases, the plasma jet is created directly during the laser action or shortly after it. Probably,

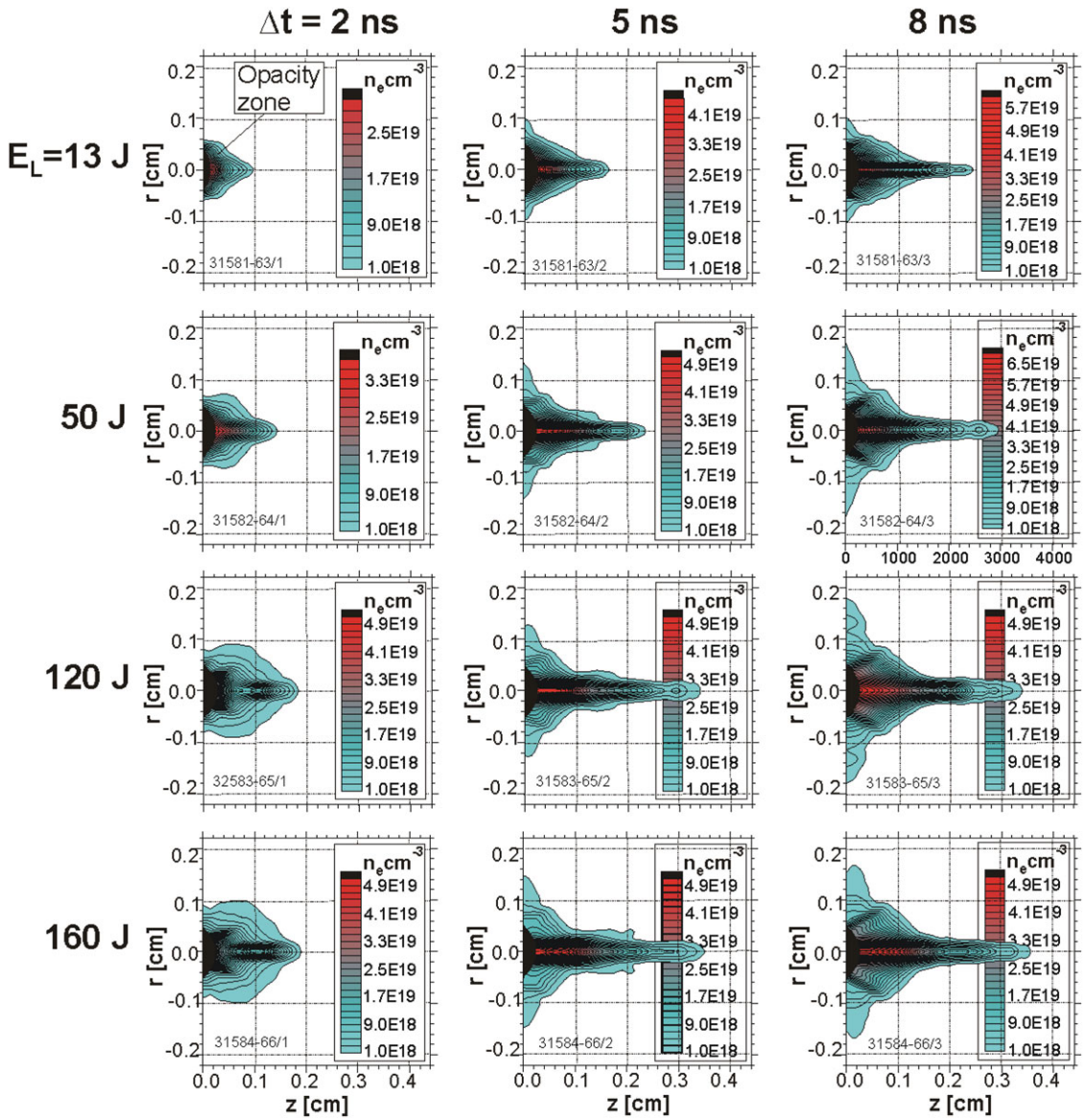

Fig. 4. Sequences of electron isodensitograms at the plasma jet forming stage. The Ag target and various laser energies.

https://doi.org/10.1017/S0263034607000547 Published online by Cambridge University Press

in the case of a relatively light target material and at very high laser energy, the plasma radiative cooling down to the temperature suitable for the jet forming takes much more time. Following this line of reasoning, the too long time of the radiative cooling of the Al plasma is responsible for the absence of plasma jets in that case (Kasperczuk *et al.*, 2006). Analogously as in the case of the smallest focal spot radii, the plasma runs away from the axial region before achieving the thermodynamic state suitable for creating the jets. Since the electron density distributions in the final period of the jet forming (see Figs. 4 and 5, $\Delta t = 5$ and 8 ns). For Ag and Ta are qualitatively similar to one another, we compare only the linear electron densities (N_e) of the Cu and Ta jets (N_e is defined as the number of electrons integrated over the cross-sectional area of the plasma stream).

In Figure 6, the N_e diagrams for a later period of the plasma jet formed on the Cu and Ta targets are presented. To show clearly the changes of the linear electron density in the jets, the high linear electron densities corresponding to the jet pedestals were partly cut off. The fronts of the pedestals are visible as steep slopes in the left part of the diagrams. One can see that the pedestals move in time with the velocities of 0.7×10^7 cm/s for the lowest laser energy, and 1.2×10^7 cm/s for the highest one.

As far as the Cu target is concerned, the linear electron density distributions along the jet at the two considered instants (5 ns and 8 ns) are similar for lower laser energies, but completely different for the highest ones. The N_e values at $\Delta t = 5$ ns are above twice as high than those at $t = 8$ ns. This is connected with the above mentioned

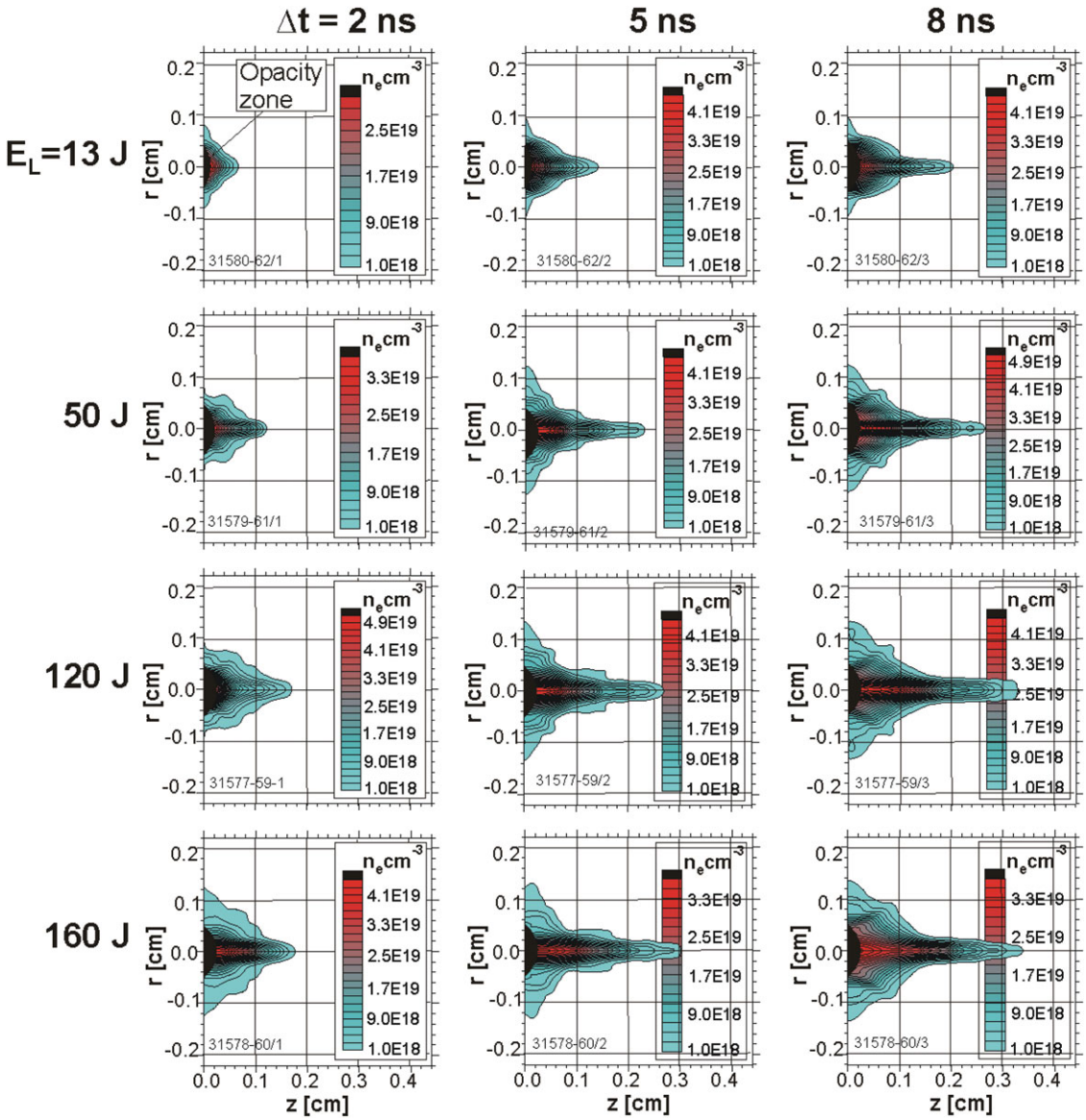

Fig. 5. Sequences of electron isodensitograms at the plasma jet forming stage. The Ta target and various laser energies.

https://doi.org/10.1017/S0263034607000547 Published online by Cambridge University Press

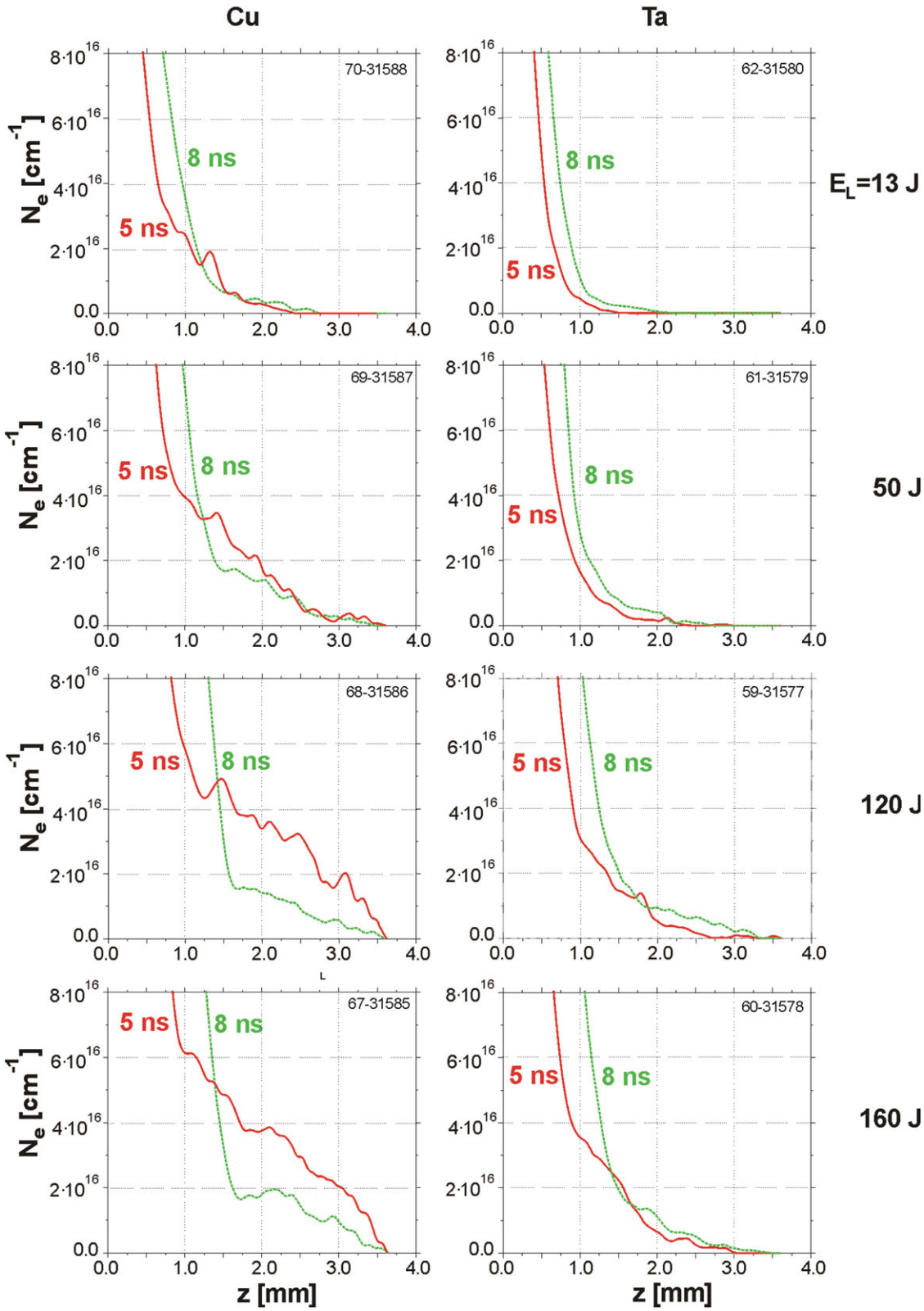

Fig. 6. The diagrams of the linear density at $\Delta t = 5$ and 8 ns for two target materials and four different laser energy values.

https://doi.org/10.1017/S0263034607000547 Published online by Cambridge University Press

different course of the plasma jet forming (via the radiative collapse) due to a great deal of the thin plasma component in the plasma stream as a whole.

In the case of the Ta target, the linear electron density distributions at $\Delta t = 5$ ns and $\Delta t = 8$ ns are very similar for all the laser energy values used. In contrast with the former case, this time the similarity of the $N_e(z)$ distributions results from the lack of plasma background.

During the period under consideration, the radial position of the 10^{18} cm^{-3} equidensity line remains approximately conserved (see Fig. 5). It means that, when assuming the free plasma expansion, the plasma flows uniformly through that equidensity contour, or that the outer thin and hot plasma envelope surrounding the jet prevents it from radial expansion. However, the plasma radiative collapse, which was observed in the case of Cu target at the highest laser energies, seems to testify that the latter mechanism can play here an essential role.

Now, we would like to pay attention to the dependence of the plasma jet production efficiency on the laser energy value. We defined the latter as the electron number in the plasma jet volume per one joule of the laser energy. This parameter, in our opinion, informs about a plasma capability to create the plasma jet. A certain problem, which appeared at computing the efficiency, was connected with determining the jet length so as to avoid including into calculations a part of the jet pedestal, the electron number of which is greater by even two orders of magnitude than that of the plasma jet. The manner of the jet length determination used is shown in Figure 7, where the linear electron density distribution $N_e(z)$ and its derivative $dN_e(z)/dz$ are drawn. It is well seen that $N_e(z)$ grows slowly along the jet from its front toward the target, increasing very sharply in the pedestal zone. The point of transition from the slow increase of $N_e(z)$ to the sharp one determines the rear end of the plasma jet. This point can be found from the derivative of $N_e(z)$. Since $N_e(z)$ changes approximately linearly along the jet, the derivative $dN_e(z)/dz$ in the jet area has a form of a horizontal line with some disturbances on it. The mean value of the derivative in the linear area is taken equal to -0.2×10^{18} cm^{-2} for all the cases under consideration. As the maximum amplitude of the disturbances amounts to 0.4×10^{18} cm^{-2}, the derivative level of -10^{18} cm^{-2} can be used at determining the positions of the jet rear end.

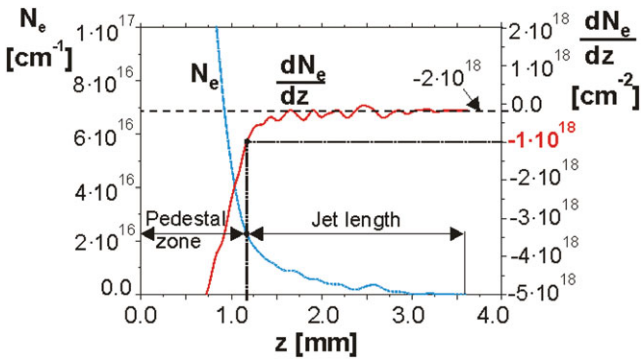

Fig. 7. Illustration of the manner of determination of the plasma jet length.

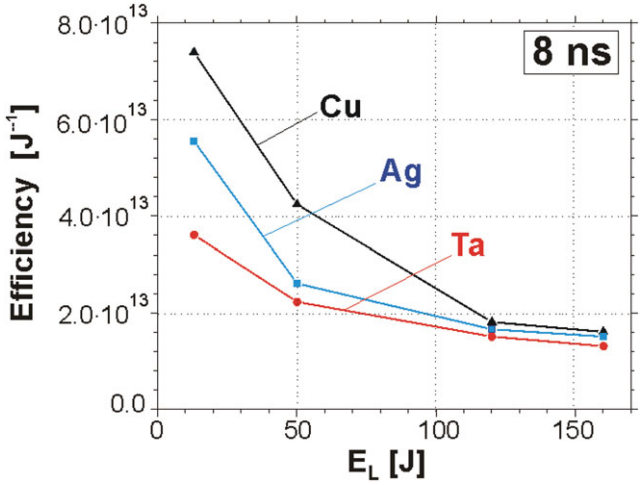

Fig. 8. Efficiency of the plasma jet production vs. the laser energy for different target materials.

The above procedure enabled to minimize errors at determining the jet production efficiency. In Figure 8, the dependences of the jet production efficiencies on the laser energy value at the final instant of the plasma jet forming ($\Delta t =$ 8 ns) for all the target materials are shown. The presented diagrams allow to state that the jet production efficiency drops with the growing laser energy. Some stabilization of that decrease of efficiency occurs at the highest laser energies, that is, above 120 J.

5. CONCLUSIONS

Our experiment has shown that the plasma jet forming is a fundamental process, which accompanies the expansion of the laser plasma produced by irradiating a massive planar target, made of material of a relatively high atomic number, with a partly defocused laser beam. At producing the plasma jets, the focal spot radius can be changed over a wide range, but its optimum value seems to be around 300 μm. The use of very large focal spot radii (600 μm) results in creation of a more complex plasma configuration.

As part of the study the laser energy was varied within a wide range. It turned out that there are no laser energy limitations for the plasma jet creation. For the entire laser energies from the range used in the experiment, the very well formed plasma jet was produced. This opens possibility of the jet production and investigation at different-scale laser facilities. Our calculations have shown that the efficiency of the jet production decreases at increasing laser energy, reaching, however, some stabilization for the highest laser energies (above 120 J). On the basis of the above results, one can conclude that the dependence of the jet velocity, diameter and electron density on the laser energy is weak. The values of these parameters do not differ too much even for the

https://doi.org/10.1017/S0263034607000547 Published online by Cambridge University Press

minimum and maximum laser energy values used in the experiment.

ACKNOWLEDGEMENTS

The work was supported in part by the Association EURATOM-IPPLM (contract No FU06-CT-2004-00081), and by the Ministry of Schools, Youth and Sports of the Czech Republic (project No LC528).

REFERENCES

Ampleford, D.J., Lebedev, S.V., Ciardi, A., Bland, S.N., Bott, S.C., Chittenden, J.P., Hall, G., Jennings, C.A., Armitage, J., Blyth, G., Christie, S. & Rutland, L. (2005). Formation of working surfaces in radioactively cooled laboratory jets. *Astrophys. Space Sci.* **298**, 241–246.

Andreev, A.A., Okada, T., Platonov, K.Y. & Toraya, S. (2004). Parameters of a fast ion jet generated by an intense ultrashort laser pulse on inhomogeneous plasma foil. *Laser Part. Beams* **22**, 431–438.

Batani, D., Dezulian, R., Redaelli, R., Benocci, R., Stabile, H., Canova, F., Desai, T., Lucchini, G., Krousky, E., Masek, K., Pfeifer, M., Skala, J., Dudzak, R., Rus, B., Ullschmied, J., Malka, V., Faure, J., Koenig, M., Limpouch, J., Nazarov, W., Pepler, D., Nagai, K., Norimatsu, T. & Nishimura, H. (2007). Recent experiments on the hydrodynamics of laser-produced plasmas conducted at the PALS laboratory. *Laser Part. Beams* **25**, 127–141.

Bellan, P.M. (2005). Miniconference on astrophysical jets. *Phys. Plasmas*. **12**, 058301-1-058301-8.

Blue, B.E., Weber, S.V., Glendinning, S.G., Lanier, N.E., Woods, D.T., Bono, M.J., Dixit, S.N., Haynam, C.A., Holder, J.P., Kalantar, D.H., MacGowan, B.J., Nikitin, A.J., Rekow, V.V., Van Wonterghem, B.M., Moses, E.I., Stry, P.E., Wilde, B.H., Hsing, W.W. & Robey, H.F. (2005). Experimental investigation of high-Mach-number 3D hydrodynamic jets at the National Ignition Facility. *Phys. Rev. Lett.* **94**, 095005-1-095005-4.

Farley, D.R., Estabrook, K.G., Glendinning, S.G., Glenzer, S.H., Remington, B.A., Shigemori, K., Stone, J.M., Wallance, R.J., Zimmerman, G.B. & Harte, J.A. (1999). Radiative jets experiments of astrophysical interest using intense lasers. *Phys. Rev. Lett.* **83**, 1982–1985.

Goldman, S.R., Caldwell, S.E., Wilke, M.D., Wilson, D.C., Cris W. Barnes, Hsing, W.W., Delamater, N.D., Schappert, G.T., Grove, J.W., Lindman, E.L., Wallance, J.M. and Weaver, R.P. (1999). Shock structuring due to fabrication joints in targets. *Phys. Plasmas* **6**, 3327–3336.

Jungwirth, K. (2005). Recent highlights of the PALS research program. *Laser Part. Beams* **23**, 177–182.

Jungwirth, K., Cejnarova, A., Juha, L., Kralikova, B., Krasa, J., Krousky, E., Krupickova, P., Laska, L., Masek, K., Prag, A., Renner, O., Rohlena, K., Rus, B., Skala, J., Straka, P. & Ullschmied, J. (2001). The Prague Asterix Laser System PALS. *Phys. Plasmas* **8**, 2495–2501.

Kasperczuk, A. & Pisarczyk, T. (2001). Application of automated interferometric system for investigation of the behaviour of a laser-produced plasma in strong external magnetic fields. *Opt. Appl.* **31**, 571–597.

Kasperczuk, A., Pisarczyk, T., Borodziuk, S., Ullschmied, J., Krousky, E., Masek, K., Rohlena, K., Skala, J. & Hora, H. (2006). Stable dense plasma jets produced at laser power densities around 10^{14} W/cm^2. *Phys. Plasmas* **13**, 062704–1–062704–8.

Nicolai, P.H., Tikhonchuk, V.T., Kasperczuk, A., Pisarczyk, T., Borodziuk, S., Rohlena, K. & Ullschmied, J. (2006). Plasma jets produced in a single laser beam interaction with a planar target. *Phys. Plasmas* **13**, 062701–1–062701–8.

Schaumann, G., Schollmeier, M.S., Rodriguez-Prieto, G., Blazevic, A., Brambrink, E., Geissel, M., Korostiy, S., Pirzadeh, P., Roth, M., Rosmej, F.B., Faenov, A.Y., Pikuz, T.A., Tsigutkin, K., Maron, Y., Tahir, N.A. & Hoffmann, D.H.H. (2005). High energy heavy ion jets emerging from laser plasma generated by long pulse laser beams from the NHELIX laser system at GSI. *Laser Part. Beams* **23**, 503–512.

Schopper, R., Ruhl, H., Kunzl, T.A. & Lesch, H. (2003). Kinetic simulation of the coherent radio emission from pulsars. *Laser Part. Beams* **21**, 109–113.

Shigemori, K., Kodama, R., Farley, D.R., Koaste, T., Estabrook, K.G., Remington, B.A., Ryutov, D.D., Ochi, Y., Azechi, H., Stone, J. & Turner, N. (2000). Experiments on radiative collapse in laser-produced plasmas relevant to astrophsical jets. *Phys. Rev. E* **62**, 8838–8841.

Sizyuk, V., Hassanein, A. & Sizyuk, T. (2007). Hollow laser self-confined plasma for extreme ultraviolet lithography and other applications. *Laser Part. Beams* **25**, 143–154.

Velarde, P., Ogando, F., Eliezer, S., Martinez-Val, Jm., Perlado, J.M. & Murakami, M. (2005). Comparison between jet collision and shell impact concepts for fast ignition. *Laser Part. Beams* **23**, 43–46.